HHS Public Access

Author manuscript

J Bioenerg Biomembr. Author manuscript; available in PMC 2018 April 01.

Published in final edited form as:

J Bioenerg Biomembr. 2017 April ; 49(2): 171–181. doi:10.1007/s10863-017-9694-z.

Analysis of an N-terminal deletion in subunit *a* of the *Escherichia coli* ATP synthase

Robert R. Ishmukhametov[1], **Jessica DeLeon-Rangel**, **Shaotong Zhu**[2], and **Steven B. Vik**[*]

Southern Methodist University, Department of Biological Sciences, Dallas, TX 75275-0376 USA

Abstract

Subunit *a* is a membrane-bound stator subunit of the ATP synthase and is essential for proton translocation. The N-terminus of subunit *a* in *E. coli* is localized to the periplasm, and contains a sequence motif that is conserved among some bacteria. Previous work has identified mutations in this region that impair enzyme activity. Here, an internal deletion was constructed in subunit *a* in which residues 6–20 were replaced by a single lysine residue, and this mutant was unable to grow on succinate minimal medium. Membrane vesicles prepared from this mutant lacked ATP synthesis and ATP-driven proton translocation, even though immunoblots showed a significant level of subunit *a*. Similar results were obtained after purification and reconstitution of the mutant ATP synthase into liposomes. The location of subunit *a* with respect to its neighboring subunits *b* and *c* was probed by introducing cysteine substitutions that were known to promote cross-linking: *a*_L207C + *c*_I55C, *a*_L121C + *b*_N4C, and *a*_T107C + *b*_V18C. The last pair was unable to form cross-links in the background of the deletion mutant. The results indicate that loss of the N-terminal region of subunit *a* does not generally disrupt its structure, but does alter interactions with subunit *b*.

Keywords

ATP synthase; F_1F_o; subunit *a*; proton translocation; rotary motor; ATPase

Introduction

ATP is synthesized during oxidative phosphorylation by a rotary enzyme called ATP synthase, or F_1F_o-ATPase. This enzyme is typically found in the membranes of mitochondria, chloroplasts, and eubacteria (For reviews see (Junge and Nelson 2015; Muench et al. 2011; Vik 2007; von Ballmoos et al. 2009)). It is composed of two parts: an F_1 sector that contains catalytic sites for ATP synthesis or hydrolysis, and an F_o sector that conducts protons across the membrane. Each sector can function as a rotary motor: a protonmotive force across the membrane drives hydrogen ion translocation (or sodium ions in some species) for ATP synthesis. Alternatively, ATP hydrolysis by F_1 can be used to generate the electrochemical gradient. The sectors are connected by two stalks. A central

[*]Corresponding author: Steven B. Vik, Department of Biological Sciences, Box 750376, Southern Methodist University, Dallas, TX 75275-0376, USA, Tel: 214-768-4228, Fax: 214-768-3955, svik@smu.edu.

[1]Present address: Clarendon Laboratory, Department of Physics, University of Oxford, OX1 3PU, UK

[2]Present address: Department of Neuroscience, University of Texas Southwestern Medical Center, Dallas, TX 75390

stalk is composed of rotary subunits, and a peripheral stalk is formed by stator subunits. In *Escherichia coli*, the enzyme consists of eight types of subunits: F_1 is formed by $\alpha_3\beta_3\gamma\delta\varepsilon$ and F_o is formed by ab_2c_{10} (Foster and Fillingame 1982).

The three-dimensional structure of the ATP synthase from *E. coli* has not been determined, but a clear picture is emerging due to a growing body of structural studies from various species. The structure of bovine mitochondrial F_1 sector was first solved by the group of Walker (Abrahams et al. 1994), and more recently a high-resolution structure of the *E. coli* F_1 was determined (Cingolani and Duncan 2011). Among the membrane subunits, the structure of the *c* subunit oligomer from several different species has been determined at high resolution (Meier et al. 2005; Pogoryelov et al. 2009; Preiss et al. 2015; Symersky et al. 2012). A 4 Å resolution structure of the intact ATP synthase from *P. denitrificans* was solved (Morales-Rios et al. 2015), but it lacked some details of the *a* and *b* subunits. Structures of intact mitochondrial ATP synthases using electron cryo-microscopy from bovine mitochondria (Zhou et al. 2015), *Polytomella* mitochondria (Allegretti et al. 2015), and *Yarrowia lipolytica* (Hahn et al. 2016) have been solved recently.

The *c* subunit from F-type ATPases is a polypeptide of about 80 residues that forms a helical hairpin. It has been shown to form ring structures, in which the number of monomers will vary according to the species: from 8 in bovine mitochondria (Watt et al. 2010) to 15 in the cyanobacterium, *Spirulina platensis* (Pogoryelov et al. 2009). Subunit *a* from *E. coli* is composed of five transmembrane helices and a sixth cytoplasmic helix, with the N-terminus in the periplasm and the C-terminus in the cytoplasm, as shown in Figure 1A (Long et al. 1998; Valiyaveetil and Fillingame 1998; Wada et al. 1999). It forms a dynamic interface with the *c*-ring during proton translocation. Recent studies (Allegretti et al. 2015; Hahn et al. 2016; Morales-Rios et al. 2015; Zhou et al. 2015) revealed that the transmembrane helices of subunit *a*, especially those that interact with the ring of *c* subunits, traverse the membrane diagonally, with little exposure at either face. The two *b* subunits in the *E. coli* enzyme each have a single transmembrane helix. They dimerize and form a fixed interface with subunit *a* in the membrane region (DeLeon-Rangel et al. 2013; Dmitriev et al. 1999; Greie et al. 2004; Motz et al. 2004), and also form the peripheral stalk that connects to F_1 subunits at the distal end of the enzyme. During ATP synthesis in *E. coli*, protons travel from the periplasm, along subunit *a* to Asp 61 of one *c* subunit. This protonation leads to rotation of the *c*-ring, which is tightly attached to the γ and ε subunits of F_1. Rotation of the asymmetric γ subunit contributes to a series of conformational changes at the catalytic sites in the α and β subunits, which are necessary for the sequential binding of ADP and P_i, formation of ATP, and release of product. The ε subunit has intrinsic inhibitory properties, which require a re-arrangement of its C-terminus in the α/β cavity (Cingolani and Duncan 2011). The catalytic subunits are connected to subunit *a* through the peripheral stalk, which contains δ and two *b* subunits. These subunits, $\alpha_3\beta_3\delta ab_2$, form the stator, against which the rotary subunits, γ-ε-c_{10}, rotate.

The primary role of subunit *a* in proton translocation is to provide access pathways for hydrogen ions to a conserved acidic residue in the *c* subunits, from both sides of the membrane. Two off-set half-channels were predicted to occur in subunit *a* (Junge et al. 1997; Vik and Antonio 1994), and have now been partially visualized by recent structural studies

(Allegretti et al. 2015; Hahn et al. 2016; Zhou et al. 2015). Accessibility studies have identified residues within subunit *a*, in the *E. coli* enzyme, that participate in formation of these half-channels (Angevine and Fillingame 2003; Angevine et al. 2003; Angevine et al. 2007; Dong and Fillingame 2010; Moore and Fillingame 2008; Steed and Fillingame 2009). The key ionic interaction occurs between Arg 210 in subunit *a* and an ionized Asp 61 of subunit *c*. Rotation of the *c*-ring during ATP synthesis follows protonation of Asp 61 in one *c* subunit, and the movement of the next *c* subunit into the proximity of Arg 210 of subunit *a*.

Residues of subunit *a* in helices H3, H4, H5 and H6 (Fig. 1A) appear to line the access channel from the periplasm to Asp 61 of subunit *c* (Angevine and Fillingame 2003; Angevine et al. 2003; Angevine et al. 2007; Dong and Fillingame 2010; Moore et al. 2008; Steed and Fillingame 2008). Other residues in H5, the cytoplasmic helix H2 and the loop between helices H4 and H5 appear to form part of the access channel to the cytoplasm. The H4-H5 loop has been cross-linked to *c* subunits using a photo-activated bi-functional cross-linker attached through monocysteines in subunit *a* (Zhang and Vik 2003a). Many residues throughout H5 and H6 have been found to form zero-length cross-links with residues in the c subunits (Jiang and Fillingame 1998; Moore and Fillingame 2008). Similarly, a residue in the cytoplasmic helix H2 (Long et al. 2002) and various residues in the H3-H4 periplasmic loop and in the membrane helix H3 (DeLeon-Rangel et al. 2013), have been cross-linked to subunit *b*. In contrast, the N-terminal residues found in the periplasm have no known role, and have not been shown to cross-link to any other subunits in the enzyme. In some bacterial species, including *E. coli*, the N-terminus of subunit *a* is unusually long, up to 40 residues, and contains a conserved sequence motif YIxHHL (Fig. 1B). The mitochondrial sequences do not align in this region, as shown previously (Hahn et al. 2016; Morales-Rios et al. 2015). Previous work from this lab (Patterson et al. 1999) showed that randomized sequences in a 9-residue region (residues 11–19) including this motif, failed to function in ATP synthesis. Mutagenesis of His 14 and His 15 to Asp led to a reduction in ATP synthase function, but also to a reduction of protein level in membranes, as detected by immunoblots, suggesting that the primary effect was on assembly. In this study, an internal deletion was constructed in the N-terminus, and the ATP synthase was isolated. In this background, interactions of subunit *a* with subunits *b* or *c* were probed by the use of sulfhydryl cross-linkers.

Materials and Methods

Materials

Restriction endonucleases were obtained from New England Biolabs, (Beverly, MA). Synthetic oligonucleotides were obtained from Eurofins MWG Operon, (Huntsville, AL). Phenol red, benzophenone-4-maleimide, carbonyl cyanide *p*-(trifluoromethoxy) phenylhydrazone (FCCP), lauryl dimethylamine oxide (LDAO) and N,N′-dicyclohexylcarbodiimide (DCCD) were purchased from Sigma (St. Louis, MO). 9-amino-6-chloro-2-methoxyacridine (ACMA) was purchased from Molecular Probes (Eugene, OR). 1,3-Propanediyl bismethanethiosulfonate (M3M) was obtained from Toronto Research Chemicals (Ontario, Canada). Materials for purification of plasmid DNA were obtained from Qiagen (Chatsworth, CA). Reagents for electrophoresis and immunoblotting were obtained from Bio-Rad (Hercules, CA). Anti-*c* antibodies were a generous gift from

Dr. Karlheinz Altendorf (Universität Osnabrück, Germany). Anti-HA antibodies, from mouse, were obtained from Roche. DNA sequencing was done by Lone Star Labs, (Houston, TX).

Plasmids, mutagenesis, growth and expression

Mutations were constructed at the N-terminal region of subunit *a* (residues 8–28) by cassette mutagenesis using plasmid pIRR2-HisHA which encodes an HA-epitope tag and a hexahistidine tag at the carboxy-terminus of subunit *a*. The plasmid pIRR2HisHA was constructed from plasmids pSBV10 (Vik and Antonio 1994) and pARP2-HisHA (Wada et al. 1999). A 0.6 kb fragment from pSBV10 was transferred to the pARP2HisHA using the ClaI and the DraIII restriction sites within the *atpB* gene. This fragment included a unique restriction site HindIII upstream of *atpB*. In the second step, a 0.4 kb fragment of the intermediate construct was replaced by a similar fragment from pARP2-HisHA using sites BsaHI and DraIII. This region includes the restriction sites necessary for the mutagenesis at the N-terminus. Mutations in pIRR2-HisHA were transferred to pFV2 (Ishmukhametov et al. 2005), the whole operon vector, using HindIII and BamHI. To produce double mutations in the genes for both subunits *a* and *c*, another plasmid, pNac, was constructed. The plasmid pFV2-HA (Bae and Vik 2009) was reduced by digesting with PpuMI and XbaI, isolating the 3.7 kb fragment, and ligating with a 15 bp linker (CTCAAGACTGGTGGT and appropriate overhangs) that regenerated the two sites. Using pNac as a template, *a*_L207C and *c*_I55C were constructed individually using the QuikChange system (Stratagene). These mutations both individually and in tandem, were transferred to pFV2-HA using PflMI and BspEI for *a*_L207C, and BspEI and PpuMI for *c*_I55C. BspEI is a unique site that occurs in DNA that codes for the HA tag at the C-terminus of subunit *a*. For cross-linking experiments, the N-terminal deletion was first transferred into pFV2-HA using HindIII and BspEI sites (0.93 kb). To combine the N-terminal deletion and the cysteine mutations, *a*_L207C and *c*_I55C, a 3.9 kb fragment containing those two mutation was ligated to a 6.3 kb fragment of pFV2-HA containing the N-terminal deletion. These fragments were generated by digestion with PflMI and MluI. A similar approach was used to transfer mutations *a*_L121C + *b*_N4C, and *a*_T107C + *b*_V18C (DeLeon-Rangel et al. 2013) to pFV2-HA containing the N-terminal deletion.

Mutations in plasmid pFV2 or pFV2-HA, which encode all eight structural genes for the ATP synthase, were used to transform the deletion strain DK8, which lacks all of the genes for the ATP synthase (Klionsky et al. 1984). Mutations were also analyzed in plasmid pIRR2 following transformation of strain RH305, which lacks subunit *a* (Hartzog and Cain 1993; Humbert et al. 1983). Growth of cultures, preparation of membrane vesicles, purification of F_1F_o, and reconstitution into liposomes were also carried out as described previously (Ishmukhametov et al. 2005; Ishmukhametov et al. 2008). Succinate minimal medium was made from minimal medium A (Miller 1972), supplemented with 0.2% succinic acid (from a stock adjusted to pH 6.4 with KOH), and 0.2 mM L-valine, L-leucine and L-isoleucine.

Functional assays

ATP hydrolysis was measured with the pH-indicator phenol red (Chance and Nishimura 1967; Zharova and Vinogradov 2006) at 37°C as described previously (Ishmukhametov et al.

2005). The enzyme was reconstituted into liposomes, using soybean asolectin at an initial lipid to protein ratio of 20 (Ishmukhametov et al. 2005). For ATP hydrolysis, the medium (2 ml) contained 10 mM HEPES/KOH, pH 8.0, 100 mM KCl, 10 mM ATP, 4 mM MgCl2, 0.1 mM EDTA, 60 μM phenol red, and 5 μM FCCP. ATP synthesis by membranes was measured with pH-indicator phenol red at 37°C following scalar proton consumption at 557 nm. Membranes were prepared as described in (Galkin et al. 2006; Ishmukhametov et al. 2008). Reactions were initiated by adding 20 mM succinate to a 2 ml cuvette containing 200 μg membrane protein in 10 mM phosphate (potassium salts) at pH 8.0, 100 mM KCl, 5 mM $MgCl_2$, 0,1 mM EDTA, 0.7 mM ADP. No ATP synthesis was observed without ADP or P_i, with the uncoupler FCCP, or after incubation with DCCD. DCCD inhibition was carried out as described previously (Ishmukhametov et al. 2005). ATP hydrolysis activity is expressed as units (μmol ATP/min) per mg protein. Measurements of ATP-dependent ACMA-fluorescence quenching were performed at pH 8.0 and at 15°C, as described previously (Ishmukhametov et al. 2005).

Analytical methods and cross-linking

Gel electrophoresis and determination of protein concentration were performed as described earlier (Ishmukhametov et al. 2005). For cross-linking studies membranes were prepared in TMG-acetate buffer (50 mM Tris acetate, 5 mM Mg acetate, 10% glycerol, pH 7.5), and including 1 mM PMSF (phenylmethylsulfonyl fluoride) and 0.1 mg/ml DNase, following published procedures (Jiang and Fillingame 1998; Moore and Fillingame 2008). *Bis*-methanethiosulfonate catalyzed-cross-linking was carried out according to the procedure of (Moore and Fillingame 2008) using 0.25 mM M3M (6.5 Å span), as previously described (DeLeon-Rangel et al. 2013). Western blots were carried out as described earlier (Zhang and Vik 2003a). Bands were quantified using NIH ImageJ software (http://rsb.info.nih.gov/ij/). Yields are expressed as the quantity of cross-linked band divided by the sum of the cross-linked and uncross-linked bands.

Results

Construction and Expression of N-terminal mutants

Monocysteine substitutions were constructed at the N-terminus of subunit *a* at each position from residue 8 to residue 28. The mutations were constructed by cassette mutagenesis (Vik et al. 1988) in the plasmid pIRR2-HisHA, and were expressed in the subunit *a* deletion strain RH305. All were capable of ATP synthesis, as indicated by growth on minimal medium supplemented with succinate, similar to other cysteine mutants in this region (Long et al. 1998; Patterson et al. 1999; Wada et al. 1999). Therefore, we turned to the examination of a deleterious internal deletion mutant in which residues 6–20 of subunit *a*, are replaced by a single lysine residue. The internal truncation was constructed in the plasmid pIRR2-HisHA, and was later transferred to pFV2, a vector that contains all 8 genes for the ATP synthase, which allows for uniform expression of the genes. The latter vector was later modified to carry the HA epitope at the C-terminus of subunit *a*, which was used for identification of cross-linked products. None of the vectors carrying the truncated gene allowed cells to grow on minimal medium with succinate as a carbon source: pIRR2-HisHA in RH305, or pFV2 in DK8, a strain deleted of the entire *atp* operon (Klionsky et al. 1984). As illustrated in Fig. 2,

the lack of growth cannot be fully explained by poor expression or poor assembly. Membrane vesicles were prepared from strain RH305 carrying the internally truncated subunit *a*, RH305/pIRR2-HisHA (Fig. 2, lane 1) and from the wild type of the same strain (lane 2). Similar results were found using constructs from DK8/pFV2-HA and from DK8/pFV2 using anti-*a* and anti-HA antibodies, respectively (results not shown). After electrophoresis, the blots were probed with anti-HA antibodies for detection of subunit *a*. In each case, a significant level of subunit *a* can be seen, typically 25–40% of the wild type level.

Enzymatic analysis of N-terminal deletion mutant

The membrane vesicles were also used to assay ATP synthesis and ATP-driven proton translocation. The results using the DK8/pFV2 strain are shown in Figures 3 and 4, and similar results were also obtained using RH305/pIRR2-HisHA (results not shown). No ATP can be synthesized by ATP synthase carrying subunit *a* with the truncated N-terminus, while the wild type construct shows a rate of about 80 nmoles ATP/min/mg protein (Fig. 3), similar to other rates reported (Ishmukhametov et al. 2008; Shah and Duncan 2015). Likewise, essentially no proton translocation can be seen from this mutant, using the energy of ATP hydrolysis (Fig. 4A). Proton translocation is indicated by the quenching of the fluorescence of ACMA due to the formation of a proton gradient across the membrane. Figure 4B shows that the membranes are capable of forming a similar proton gradient if NADH is used as the source of energy. Furthermore, as shown in Figure 4C, if the membranes are stripped of F_1, the wild type cannot maintain a proton gradient during NADH oxidation, whereas the mutant retains this ability. This can be explained by a rapid proton leak through the wild type F_o, and a proton impermeable F_o, in the case of the mutant.

Finding no evidence of energy-linked function by the truncated subunit *a* mutant, we next examined the ability of the membrane vesicles to hydrolyze ATP. The rate of ATP hydrolysis by the wild type membranes is about twice that of the subunit *a* mutant (Fig. 5A). When the assay was repeated in the presence of 0.4% LDAO, which can relieve intrinsic inhibition of the F_1-ATPase, the rates are essentially the same (Fig. 5B). The wild type was stimulated about 2.75 fold, while the truncated mutant was stimulated about 6 fold. This indicates that the amount of F_1 bound to the membranes is about the same, even though the level of subunit *a* is somewhat lower in the case of the mutant. Partial complexes of ATP synthase must have formed that lack subunit *a*, and perhaps other subunits as well. Finally, the sensitivity of ATP hydrolysis to inhibition by DCCD was measured. The ability of DCCD to inhibit ATP hydrolysis is generally an indication of tight coupling between the F_1 and F_o sectors, and of a properly assembled F_o. Wild type membranes show a typical 70 % inhibition of ATP hydrolysis after pre-treatment with 50 μM DCCD (Fig. 5C). In contrast, the truncation mutant shows only about 5% inhibition after the same treatment (Fig. 5D).

The results at this point suggested that the ATP synthase in membrane preparations containing the subunit *a*Δ6–20 mutation functions poorly. Therefore, the enzyme was purified from the membranes of the DK8/pFV2 strain via the His-tag at the N-terminus of the β subunit, in order to verify the level of subunit *a* that is incorporated into the ATP

synthase. As shown in Figure 6, the level of subunit *a* was low, only about 20% of the wild type level. The relative levels of δ and *b* subunits from the *a*Δ6–20 strain also appeared to be lower than that found in the wild type enzyme, although this is dependent on the staining technique. Subunit *a* stains more intensely with silver staining due to its hydrophobic nature. The *c* subunits were not visualized in this gel, *i.e.*, were run off the gel in order to enhance resolution of the larger subunits. The mutant F_1F_o reconstituted into proteoliposomes failed to exhibit ATP-driven proton translocation, as indicated by fluorescence quenching of ACMA, although this was observed with the wild type enzyme (results not shown, (Ishmukhametov et al. 2008)). With the reconstituted enzymes the rates of ATP hydrolysis by both constructs were essentially the same, and the stimulation by LDAO was also the same, about 3-fold (results not shown). This indicates that the reduced level of subunit *a*, or the N-terminal truncation itself, are not sufficient to cause inhibition of ATP hydrolysis. Finally, the sensitivity of ATP hydrolysis to DCCD was tested in the purified enzyme. In this case, the results were the same as with the membrane bound enzyme. The wild type enzyme showed about 70% sensitivity, while the enzyme with the N-terminal deletion in subunit *a* was only about 5% sensitive (results not shown).

The lack of DCCD sensitivity suggested that either *a*-*c* subunits were not properly interacting, or that F_1-F_o interactions were disturbed. To identify possible interactions between the N-terminus of subunit *a* and other subunits, cross-linking experiments were carried out with the monocysteine substitutions that had been constructed at each position from residue 8 to residue 28. In previous work (DeLeon-Rangel et al. 2013) we had shown that the photo-activated cross-linker, benzophenone-4-maleimide, could form *a*-*b* cross-links from periplasmic cysteine-substituted residues in subunit *a*, such as residues 129 and 146. The analysis here found that none of the cysteines at the N-terminus of subunit *a* generated cross-linked products (results not shown).

Analysis of subunit assembly by cross-linking

To test whether the subunit *a* in the deletion mutant was properly positioned with respect to subunit *c*, we relied upon a previous study by Jiang and Fillingame (Jiang and Fillingame 1998) in which they showed that *a*_L207C and *c*_I55C can be disulfide-cross-linked. Residue Leu 207 is proximate to key residue Arg 210, and is colored magenta in Figure 1B. This pair of mutations was combined with the N-terminal deletion in subunit *a* in the pFV2-HA construct, and cross-linking reactions were carried out in membrane vesicles in the DK8 strain, using the *bis*-methanethiosulfonate cross-linker, M3M. In three membrane preparations, the wild type cross-link yield was 47% (± 7) while the truncated mutant was 48% (±10), indicating no significant difference between the two. A representative blot is shown in Figure 7. A band migrating above the *a*-*c* product in the untreated lanes is an artifact, and is marked by an x.

In recent work (DeLeon-Rangel et al. 2013) we had found several pairs of cysteine substitutions in subunits *a* and *b* that could form disulfide cross-links. Therefore, we tried to test the effect of the deletion mutant on the interactions of subunits *a* and *b*. Two of these pairs were tested with the N-terminal deletion in subunit *a:* *a*_L121C + *b*_N4C, and *a*_T107C + *b*_V18C. Residues Leu 121 and Thr 107 are shown in Figure 1A, colored blue.

The first pair, *a*_L121C + *b*_N4C, is expected to be found near the periplasmic surface, while the second pair, *a*_T107C + *b*_V18C, should be found within the membrane towards the cytoplasm. The mutations were transferred to the pFV2-HA construct, and analyzed in the DK8 background strain. The cross-linking reactions were carried out in membrane vesicles using the *bis*-methanethiosulfonate cross-linker, M3M, and a representative blot is shown in Figure 8. The results show that the cross-link between *a*_L121C and *b*_N4C, near the periplasmic surface, appears to form normally in the background of the N-terminal deletion. In contrast, the cross-link between *a*_T107C and *b*_V18C, is greatly diminished, or does not form. The cross-linking results suggest that the absence of the N-terminal residues 6–20 of subunit *a* does not affect the interactions of subunit *a* with the ring of *c* subunits, but it does affect interactions with at least one of the *b* subunits.

Homology model

In order to visualize the location of the N-terminus of subunit *a*, a homology model was obtained using the Phyre2 suite (Kelley et al. 2015), shown in Figure 9. Since the model was built primarily using the bovine enzyme, which has a single subunit *b* with 2 transmembrane spans, and a single *d* subunit with one transmembrane span, some details might not be accurately modeled. Overall, the model is consistent with surface labeling studies (Long et al. 2002; Long et al. 1998; Patterson et al. 1999; Valiyaveetil and Fillingame 1998; Wada et al. 1999; Zhang and Vik 2003a; Zhang and Vik 2003b). The model shows a helical segment at the N-terminus, roughly corresponding to the deleted segment colored blue, that is wedged between transmembrane helices of subunit *a*. This helix is based on secondary-structure predictions (Jones 1999), since the bovine protein has no homologous region. The N-terminal helix appears to be found near where *b* subunits would be located, rather than near the interface with the ring of *c* subunits, as marked by the presence of Arg 210, colored magenta.

4. Discussion

Cysteine-scanning mutagenesis of the N-terminus of subunit *a* indicated that none of the residues in this conserved region are critical for function. All single-cysteine mutants could still grow using succinate as sole carbon source, indicating that the ATP synthase was active. Only when the most highly conserved 15 residues (6–20) were replaced by a single lysine was function lost. These results support those from an earlier, but more limited, study directed at His 14 and His 15 (Patterson et al. 1999). Mutation of residues 14, 15, 17, and 18 to cysteine had only small effects on enzyme function. That study also showed that when residues 11–19 were randomly mutagenized in a group, none of the resulting mutants could grow on succinate minimal medium. Those results were comparable to the findings here concerning the deletion mutant. In another much earlier study (Lewis and Simoni 1992), deletion of residues 2–35, representing the entire periplasmic segment in subunit *a,* was shown to result in the same growth phenotype. In that case, it is likely that the level of subunit *a* in the membranes was greatly diminished, but antibodies were not available then to verify that.

In the current study, the analysis was focused on the internally-deleted subunit *a*. Its expression level in membrane preparations was estimated by immunoblotting, and found to be about 25–40% of the wild type protein. Previous studies (Ono et al. 2004; Vik and Simoni 1987) had shown that the ATP synthase can assemble without subunit *a*. More recently, it was shown that subunit *a* can enter a pre-assembled complex of the other subunits, and produce a functional enzyme (Brockmann et al. 2013). The level of subunit *a* seen here is not low enough to account for the total lack of ATP synthesis, ATP-driven proton translocation, and loss of sensitivity of ATP hydrolysis to DCCD. Since subunit *a* is specifically targeted by the FtsH protease in *E. coli*, it is likely that any subunit *a* not properly incorporated into the ATP synthase will be rapidly degraded (Akiyama et al. 1996), which would account for the reduced levels seen here. In membrane vesicles the ATP hydrolysis activity of the truncated mutant is lower than that of the wild type, but after addition of LDAO to the membranes, both rates are similar. LDAO is known to activate the *E. coli* F_1-ATPase activity (Dunn et al. 1990; Lötscher et al. 1984; Peskova and Nakamoto 2000). This activation suggests that the same level of F_1-ATPase is present in both membranes, and that the deficiency of subunit *a* due to the truncation results in aberrant ATP synthase that is partially inhibited.

To clarify this issue, the enzyme was purified and subjected to a similar series of assays. First, the subunit composition of the enzyme revealed by SDS gel electrophoresis, showed that the level of subunit *a* was no more than 25% of the wild type level. In addition, the peripheral stalk proteins, *b* and δ, were also reduced relative to the wild type. The isolated enzyme, after incorporation into proteoliposomes, showed no ATP-driven proton translocation, nor sensitivity of ATP hydrolysis to DCCD. But, in contrast to the membrane preparations, ATP hydrolysis rates of the truncated subunit *a* and wild type enzyme were the same, with or without addition of LDAO. It appears that the inhibited form of the ATPase is activated during the isolation procedure.

Possible roles for the N-terminus of subunit *a* include the following: membrane integration of subunit *a*, formation of proper subunit interactions with *b* or *c* subunits, and a direct role in proton translocation. Although the N-terminus contains a highly-conserved pair of His residues (Fig. 1A), the analysis of the single cysteine substitutions at each position makes an essential role in proton translocation unlikely. Mutation to Cys had little effect on cell growth properties. Furthermore, the simple loss of the ability to translocate protons should not cause a total loss of sensitivity to DCCD (Cain and Simoni 1988; Valiyaveetil and Fillingame 1997; Vik et al. 1988).

Subunit *a* requires the YidC protein for its incorporation into the membrane (Kol et al. 2009; Yi et al. 2003), and so it is possible that the N-terminal deletion impairs that interaction. It is difficult to detect subunit *a* that is not incorporated into the ATP synthase, and it has been demonstrated that subunit *a* cannot survive without the presence of both *b* and *c* subunits in an F_o complex (Hermolin and Fillingame 1995). That observation is likely explained by the fact that subunit *a* is a substrate of the protease FtsH (Akiyama et al. 1996). In any case, poor incorporation of subunit *a* into the membrane cannot account for the total loss of function seen, because some subunit *a* was always seen in our membrane fractions or isolated

complexes. So, while membrane integration might be part of the role of the N-terminus, to explain the results here, there must also be another role.

The remaining possibility is that the truncated subunit *a* has altered interactions with *b* or *c* subunits, which could explain both the loss of function and the reduced level of subunit *a*. This was tested in the case of subunit *c* by cross-linking with M3M. The yield of cross-linking between *a*_L207C and *c*_I55C was not affected by the N-terminal deleted residues. In the *E. coli* enzyme, the interface between the ring of *c* subunits and subunit *a* is thought to involve primarily the last 2 transmembrane helices (H5 and H6) of subunit *a* (Jiang and Fillingame 1998; Moore and Fillingame 2008), and the preceding cytoplasmic loop of H4-H5 (Zhang and Vik 2003a). Those results are now supported by the electron cryo-microscopy studies of mitochondrial enzymes (Allegretti et al. 2015; Hahn et al. 2016; Zhou et al. 2015), and the homology model of subunit *a* (Fig. 9). Therefore, it seems unlikely that the N-terminus of subunit *a* interacts directly with the *c*-ring.

That leaves the possibility that the N-terminal deletion in subunit *a* affects its interactions with *b* subunits. The phenotype of the truncated subunit *a* mutant is remarkably similar to that of the *b*_G9D mutant, first isolated over 30 years ago (Jans et al. 1985; Porter et al. 1985). Also, that mutant cannot grow on succinate minimal media, and its membranes are not capable of ATP-driven proton translocation. The membranes were shown to have reduced rates of ATP hydrolysis, and partial (40%) sensitivity to DCCD (Kumamoto and Simoni 1986). The truncated subunit *a* mutant described here differed primarily in that it had even lower sensitivity to DCCD (about 5%). Furthermore, partial purification of the ATP synthase carrying the *b*_G9D mutation showed reduced levels of subunit *a* (Vik and Simoni 1987), very similar to the truncated subunit *a* mutant. In this work, two different sites of cross-linking between subunits *a* and *b* were shown to have different outcomes. The pair of residues near the periplasmic surface, *a*_L121C and *b*_N4C, retained the ability to form cross-links in the background of the N-terminal deletion. It is possible that *b*_N4C is able to find its partner residue, even in an altered environment, due to flexibility at the N-terminus of subunit *b*. In the case of *a*_T107C and *b*_V18C, the inability to form a cross-link could be indicative of one or both *b* subunits that are displaced relative to subunit *a* near the cytoplasmic surface. That could have profound effects on the interactions of *b* subunits with δ, at the crown of the ATP synthase. In this way, a deletion in the N-terminus of subunit *a* could affect the structure of the stator/peripheral stalk, leading to a weakening/slipping of the stator and the partial loss of *a*-*b*-δ subunits. This would explain the inability to drive proton translocation and the loss of DCCD sensitivity. More generally, one can predict that in ATP synthases the structure of the N-terminus of subunit *a* is likely to vary among different species according to the different types of stator structures.

Acknowledgments

This work was supported by grants from the NIH (GM-40508) and the Welch Foundation (N-1378) to S.B.V.

This work was supported by grant R01GM40508 from the National Institutes of Health (USA). The authors thank SMU students Uju Rochas, Mai Bedair and Damilola Salako for constructing some of the plasmids necessary for the final experiments.

References

Abrahams JP, Leslie AG, Lutter R, Walker JE. Structure at 2.8 Å resolution of F_1-ATPase from bovine heart mitochondria. Nature. 1994; 370:621–628. DOI: 10.1038/370621a0 [PubMed: 8065448]

Akiyama Y, Kihara A, Ito K. Subunit *a* of proton ATPase F_o sector is a substrate of the *FtsH* protease in *Escherichia coli*. FEBS Lett. 1996; 399:26–28. [PubMed: 8980112]

Allegretti M, Klusch N, Mills DJ, Vonck J, Kuhlbrandt W, Davies KM. Horizontal membrane-intrinsic alpha-helices in the stator *a*-subunit of an F-type ATP synthase. Nature. 2015; 521:237–240. DOI: 10.1038/nature14185 [PubMed: 25707805]

Angevine CM, Fillingame RH. Aqueous access channels in subunit *a* of rotary ATP synthase. J Biol Chem. 2003; 278:6066–6074. DOI: 10.1074/jbc.M210199200 [PubMed: 12473663]

Angevine CM, Herold KA, Fillingame RH. Aqueous access pathways in subunit *a* of rotary ATP synthase extend to both sides of the membrane. Proc Natl Acad Sci U S A. 2003; 100:13179–13183. DOI: 10.1073/pnas.2234364100 [PubMed: 14595019]

Angevine CM, Herold KA, Vincent OD, Fillingame RH. Aqueous access pathways in ATP synthase subunit *a* Reactivity of cysteine substituted into transmembrane helices 1, 3, and 5. J Biol Chem. 2007; 282:9001–9007. DOI: 10.1074/jbc.M610848200 [PubMed: 17234633]

Bae L, Vik SB. A more robust version of the Arginine 210-switched mutant in subunit *a* of the *Escherichia coli* ATP synthase. Biochim Biophys Acta. 2009; 1787:1129–1134. DOI: 10.1016/j.bbabio.2009.03.022 [PubMed: 19362069]

Brockmann B, Koop Genannt Hoppmann KD, Strahl H, Deckers-Hebestreit G. Time-delayed in vivo assembly of subunit *a* into preformed *Escherichia coli* F_oF_1 ATP synthase. J Bacteriol. 2013; 195:4074–4084. DOI: 10.1128/JB.00468-13 [PubMed: 23836871]

Cain BD, Simoni RD. Interaction between Glu-219 and His-245 within the *a* subunit of F_1F_o-ATPase in *Escherichia coli*. J Biol Chem. 1988; 263:6606–6612. [PubMed: 2896197]

Chance B, Nishimura M. Sensitive measurements of changes of hydrogen ion concentration. Methods Enzymol. 1967; 10:641–650.

Cingolani G, Duncan TM. Structure of the ATP synthase catalytic complex (F_1) from *Escherichia coli* in an autoinhibited conformation. Nat Struct Mol Biol. 2011; 18:701–707. DOI: 10.1038/nsmb.2058 [PubMed: 21602818]

DeLeon-Rangel J, Ishmukhametov RR, Jiang W, Fillingame RH, Vik SB. Interactions between subunits *a* and *b* in the rotary ATP synthase as determined by cross-linking. FEBS Lett. 2013; 587:892–897. DOI: 10.1016/j.febslet.2013.02.012 [PubMed: 23416299]

Dmitriev O, Jones PC, Jiang W, Fillingame RH. Structure of the membrane domain of subunit *b* of the *Escherichia coli* F_0F_1 ATP synthase. J Biol Chem. 1999; 274:15598–15604. [PubMed: 10336456]

Dong H, Fillingame RH. Chemical reactivities of cysteine substitutions in subunit *a* of ATP synthase define residues gating H+ transport from each side of the membrane. J Biol Chem. 2010; 285:39811–39818. DOI: 10.1074/jbc.M110.175844 [PubMed: 20943664]

Dunn SD, Tozer RG, Zadorozny VD. Activation of *Escherichia coli* F_1-ATPase by lauryldimethylamine oxide and ethylene glycol: relationship of ATPase activity to the interaction of the ε and β subunits. Biochemistry. 1990; 29:4335–4340. [PubMed: 2140947]

Foster DL, Fillingame RH. Stoichiometry of subunits in the H^+-ATPase complex of *Escherichia coli*. J Biol Chem. 1982; 257:2009–2015. [PubMed: 6460031]

Galkin MA, Ishmukhametov RR, Vik SB. A functionally inactive, cold-stabilized form of the *Escherichia coli* F_1F_o ATP synthase. Biochim Biophys Acta. 2006; 1757:206–214. DOI: 10.1016/j.bbabio.2006.02.011 [PubMed: 16581013]

Greie JC, Heitkamp T, Altendorf K. The transmembrane domain of subunit *b* of the *Escherichia coli* F_1F_o ATP synthase is sufficient for H+-translocating activity together with subunits *a* and *c*. Eur J Biochem. 2004; 271:3036–3042. DOI: 10.1111/j.1432-1033.2004.04235.x [PubMed: 15233800]

Hahn A, Parey K, Bublitz M, Mills DJ, Zickermann V, Vonck J, Kuhlbrandt W, Meier T. Structure of a complete ATP synthase dimer reveals the molecular basis of inner mitochondrial membrane morphology. Mol Cell. 2016; 63:445–456. DOI: 10.1016/j.molcel.2016.05.037 [PubMed: 27373333]

Hartzog PE, Cain BD. Mutagenic analysis of the *a* subunit of the F_1F_o ATP synthase in *Escherichia coli*: Gln-252 through Tyr-263. J Bacteriol. 1993; 175:1337–1343. [PubMed: 8383111]

Hermolin J, Fillingame RH. Assembly of F_o sector of *Escherichia coli* H^+ ATP synthase. Interdependence of subunit insertion into the membrane. J Biol Chem. 1995; 270:2815–2817. [PubMed: 7852354]

Humbert R, Brusilow WS, Gunsalus RP, Klionsky DJ, Simoni RD. *Escherichia coli* mutants defective in the *uncH* gene. J Bacteriol. 1983; 153:416–422. [PubMed: 6294057]

Ishmukhametov RR, Galkin MA, Vik SB. Ultrafast purification and reconstitution of His-tagged cysteine-less *Escherichia coli* F_1F_o ATP synthase. Biochim Biophys Acta. 2005; 1706:110–116. DOI: 10.1016/j.bbabio.2004.09.012 [PubMed: 15620371]

Ishmukhametov RR, Pond JB, Al-Huqail A, Galkin MA, Vik SB. ATP synthesis without R210 of subunit *a* in the *Escherichia coli* ATP synthase. Biochim Biophys Acta. 2008; 1777:32–38. DOI: 10.1016/j.bbabio.2007.11.004 [PubMed: 18068111]

Jans DA, Hatch L, Fimmel AL, Gibson F, Cox GB. Complementation between *uncF* alleles affecting assembly of the F_1F_o-ATPase complex of *Escherichia coli*. J Bacteriol. 1985; 162:420–426. [PubMed: 2858470]

Jiang W, Fillingame RH. Interacting helical faces of subunits *a* and *c* in the F_1F_o ATP synthase of *Escherichia coli* defined by disulfide cross-linking. Proc Natl Acad Sci U S A. 1998; 95:6607–6612. [PubMed: 9618459]

Jones DT. Protein secondary structure prediction based on position-specific scoring matrices. J Mol Biol. 1999; 292:195–202. DOI: 10.1006/jmbi.1999.3091 [PubMed: 10493868]

Junge W, Lill H, Engelbrecht S. ATP synthase: an electrochemical transducer with rotatory mechanics. Trends Biochem Sci. 1997; 22:420–423. [PubMed: 9397682]

Junge W, Nelson N. ATP synthase. Annu Rev Biochem. 2015; 84:631–657. DOI: 10.1146/annurev-biochem-060614-034124 [PubMed: 25839341]

Kelley LA, Mezulis S, Yates CM, Wass MN, Sternberg MJ. The Phyre2 web portal for protein modeling, prediction and analysis. Nat Protoc. 2015; 10:845–858. DOI: 10.1038/nprot.2015.053 [PubMed: 25950237]

Klionsky DJ, Brusilow WS, Simoni RD. In vivo evidence for the role of the ε subunit as an inhibitor of the proton-translocating ATPase of *Escherichia coli*. J Bacteriol. 1984; 160:1055–1060. [PubMed: 6238948]

Kol S, Majczak W, Heerlien R, van der Berg JP, Nouwen N, Driessen AJ. Subunit *a* of the F_1F_o ATP synthase requires YidC and SecYEG for membrane insertion. J Mol Biol. 2009; 390:893–901. DOI: 10.1016/j.jmb.2009.05.074 [PubMed: 19497329]

Kumamoto CA, Simoni RD. Genetic evidence for interaction between the *a* and *b* subunits of the F_o portion of the *Escherichia coli* proton translocating ATPase. J Biol Chem. 1986; 261:10037–10042. [PubMed: 2874136]

Lewis MJ, Simoni RD. Deletions in hydrophilic domains of subunit *a* from the *Escherichia coli* F_1F_o-ATP synthase interfere with membrane insertion or F_o assembly. J Biol Chem. 1992; 267:3482–3489. [PubMed: 1531341]

Long JC, DeLeon-Rangel J, Vik SB. Characterization of the first cytoplasmic loop of subunit *a* of the *Escherichia coli* ATP synthase by surface labeling, cross-linking, and mutagenesis. J Biol Chem. 2002; 277:27288–27293. DOI: 10.1074/jbc.M202118200 [PubMed: 12021273]

Long JC, Wang S, Vik SB. Membrane topology of subunit *a* of the F_1F_o ATP synthase as determined by labeling of unique cysteine residues. J Biol Chem. 1998; 273:16235–16240. [PubMed: 9632682]

Lötscher HR, de Jong C, Capaldi RA. Interconversion of high and low adenosinetriphosphatase activity forms of *Escherichia coli* F_1 by the detergent lauryldimethylamine oxide. Biochemistry. 1984; 23:4140–4143. [PubMed: 6237684]

Meier T, Polzer P, Diederichs K, Welte W, Dimroth P. Structure of the rotor ring of F-Type Na^+-ATPase from *Ilyobacter tartaricus*. Science. 2005; 308:659–662. DOI: 10.1126/science.1111199 [PubMed: 15860619]

Miller, JH. Experiments in Molecular Genetics. Cold Spring Harbor Laboratory Press; Cold Spring Harbor, New York: 1972.

Moore KJ, Angevine CM, Vincent OD, Schwem BE, Fillingame RH. The cytoplasmic loops of subunit *a* of *Escherichia coli* ATP synthase may participate in the proton translocating mechanism. J Biol Chem. 2008; 283:13044–13052. DOI: 10.1074/jbc.M800900200 [PubMed: 18337242]

Moore KJ, Fillingame RH. Structural interactions between transmembrane helices 4 and 5 of subunit *a* and the subunit *c* ring of *Escherichia coli* ATP synthase. J Biol Chem. 2008; 283:31726–31735. DOI: 10.1074/jbc.M803848200 [PubMed: 18786930]

Morales-Rios E, Montgomery MG, Leslie AG, Walker JE. Structure of ATP synthase from *Paracoccus denitrificans* determined by X-ray crystallography at 4.0 A resolution. Proc Natl Acad Sci U S A. 2015; 112:13231–13236. DOI: 10.1073/pnas.1517542112 [PubMed: 26460036]

Motz C, Hornung T, Kersten M, McLachlin DT, Dunn SD, Wise JG, Vogel PD. The subunit *b* dimer of the F_oF_1-ATP synthase: interaction with F_1-ATPase as deduced by site-specific spin-labeling. J Biol Chem. 2004; 279:49074–49081. DOI: 10.1074/jbc.M404543200 [PubMed: 15339903]

Muench SP, Trinick J, Harrison MA. Structural divergence of the rotary. ATPases Q Rev Biophys. 2011; 44:311–356. DOI: 10.1017/S0033583510000338 [PubMed: 21426606]

Ono S, Sone N, Yoshida M, Suzuki T. ATP synthase that lacks F_o*a*-subunit: isolation, properties, and indication of F_ob_2-subunits as an anchor rail of a rotating *c*-ring. J Biol Chem. 2004; 279:33409–33412. DOI: 10.1074/jbc.M404993200 [PubMed: 15175330]

Patterson AR, Wada T, Vik SB. His15 of subunit *a* of the *Escherichia coli* ATP synthase is important for the structure or assembly of the membrane sector F_o. Arch Biochem Biophys. 1999; 368:193–197. DOI: 10.1006/abbi.1999.1306 [PubMed: 10415127]

Peskova YB, Nakamoto RK. Catalytic control and coupling efficiency of the *Escherichia coli* F_oF_1 ATP synthase: influence of the F_o sector and ε subunit on the catalytic transition state. Biochemistry. 2000; 39:11830–11836. [PubMed: 10995251]

Pogoryelov D, Yildiz O, Faraldo-Gomez JD, Meier T. High-resolution structure of the rotor ring of a proton-dependent ATP synthase. Nat Struct Mol Biol. 2009; 16:1068–1073. DOI: 10.1038/nsmb.1678 [PubMed: 19783985]

Porter AC, Kumamoto C, Aldape K, Simoni RD. Role of the *b* subunit of the *Escherichia coli* proton-translocating ATPase. A mutagenic analysis. J Biol Chem. 1985; 260:8182–8187. [PubMed: 2861200]

Preiss L, Langer JD, Yildiz O, Eckhardt-Strelau L, Guillemont JE, Koul A, Meier T. Structure of the mycobacterial ATP synthase F rotor ring in complex with the anti-TB drug bedaquiline. Sci Adv. 2015; 1:e1500106.doi: 10.1126/sciadv.1500106 [PubMed: 26601184]

Shah NB, Duncan TM. Aerobic growth of *Escherichia coli* is reduced, and ATP synthesis is selectively inhibited when five C-terminal residues are deleted from the subunit of ATP synthase. J Biol Chem. 2015; 290:21032–21041. DOI: 10.1074/jbc.M115.665059 [PubMed: 26160173]

Steed PR, Fillingame RH. Subunit *a* facilitates aqueous access to a membrane-embedded region of subunit *c* in *Escherichia coli* F_1F_0 ATP synthase. J Biol Chem. 2008; 283:12365–12372. DOI: 10.1074/jbc.M800901200 [PubMed: 18332132]

Steed PR, Fillingame RH. Aqueous accessibility to the transmembrane regions of subunit *c* of the *Escherichia coli* F_1F_0 ATP synthase. J Biol Chem. 2009; 284:23243–23250. DOI: 10.1074/jbc.M109.002501 [PubMed: 19542218]

Symersky J, Pagadala V, Osowski D, Krah A, Meier T, Faraldo-Gomez JD, Mueller DM. Structure of the c_{10} ring of the yeast mitochondrial ATP synthase in the open conformation. Nat Struct Mol Biol. 2012; 19:485–491. S481. DOI: 10.1038/nsmb.2284 [PubMed: 22504883]

Valiyaveetil FI, Fillingame RH. On the role of Arg-210 and Glu-219 of subunit *a* in proton translocation by the *Escherichia coli* F_oF_1-ATP synthase. J Biol Chem. 1997; 272:32635–32641. [PubMed: 9405480]

Valiyaveetil FI, Fillingame RH. Transmembrane topography of subunit *a* in the *Escherichia coli* F_1F_0 ATP synthase. J Biol Chem. 1998; 273:16241–16247. [PubMed: 9632683]

Vik, SB. ATP synthesis by oxidative phosphorylation. In: Böck, A., et al., editors. EcoSal—*Escherichia coli* and *Salmonella*: Cellular and molecular biology. ASM Press; Washington D.C: 2007.

Vik SB, Antonio BJ. A mechanism of proton translocation by F_1F_o ATP synthases suggested by double mutants of the *a* subunit. J Biol Chem. 1994; 269:30364–30369. [PubMed: 7982950]

Vik SB, Cain BD, Chun KT, Simoni RD. Mutagenesis of the *a* subunit of the F_1F_o-ATPase from *Escherichia coli* Mutations at Glu-196, Pro-190, and Ser-199. J Biol Chem. 1988; 263:6599–6605. [PubMed: 2896196]

Vik SB, Simoni RD. F_1F_o-ATPase from *Escherichia coli* with mutant F_o subunits. Partial purification and immunoprecipitation of F_1F_o complexes. J Biol Chem. 1987; 262:8340–8346. [PubMed: 2885319]

von Ballmoos C, Wiedenmann A, Dimroth P. Essentials for ATP synthesis by F_1F_o ATP synthases. Annu Rev Biochem. 2009; 78:649–672. DOI: 10.1146/annurev.biochem.78.081307.104803 [PubMed: 19489730]

Wada T, Long JC, Zhang D, Vik SB. A novel labeling approach supports the five-transmembrane model of subunit *a* of the *Escherichia coli* ATP synthase. J Biol Chem. 1999; 274:17353–17357. [PubMed: 10358096]

Watt IN, Montgomery MG, Runswick MJ, Leslie AG, Walker JE. Bioenergetic cost of making an adenosine triphosphate molecule in animal mitochondria. Proc Natl Acad Sci U S A. 2010; 107:16823–16827. DOI: 10.1073/pnas.1011099107 [PubMed: 20847295]

Yi L, Jiang F, Chen M, Cain B, Bolhuis A, Dalbey RE. *YidC* is strictly required for membrane insertion of subunits *a* and *c* of the F_1F_o ATP synthase and *SecE* of the *SecYEG* translocase. Biochemistry. 2003; 42:10537–10544. DOI: 10.1021/bi034309h [PubMed: 12950181]

Zhang D, Vik SB. Close proximity of a cytoplasmic loop of subunit *a* with *c* subunits of the ATP synthase from *Escherichia coli*. J Biol Chem. 2003a; 278:12319–12324. DOI: 10.1074/jbc.M212413200 [PubMed: 12525480]

Zhang D, Vik SB. Helix packing in subunit *a* of the *Escherichia coli* ATP synthase as determined by chemical labeling and proteolysis of the cysteine-substituted protein. Biochemistry. 2003b; 42:331–337. DOI: 10.1021/bi026649t [PubMed: 12525160]

Zharova TV, Vinogradov AD. Requirement of medium ADP for the steady-state hydrolysis of ATP by the proton-translocating *Paracoccus denitrificans* F_oF_1-ATP synthase. Biochim Biophys Acta. 2006; 1757:304–310. DOI: 10.1016/j.bbabio.2006.03.001 [PubMed: 16730637]

Zhou A, Rohou A, Schep DG, Bason JV, Montgomery MG, Walker JE, Grigorieff N, Rubinstein JL. Structure and conformational states of the bovine mitochondrial ATP synthase by cryo-EM. Elife. 2015; 4:e10180.doi: 10.7554/eLife.10180 [PubMed: 26439008]

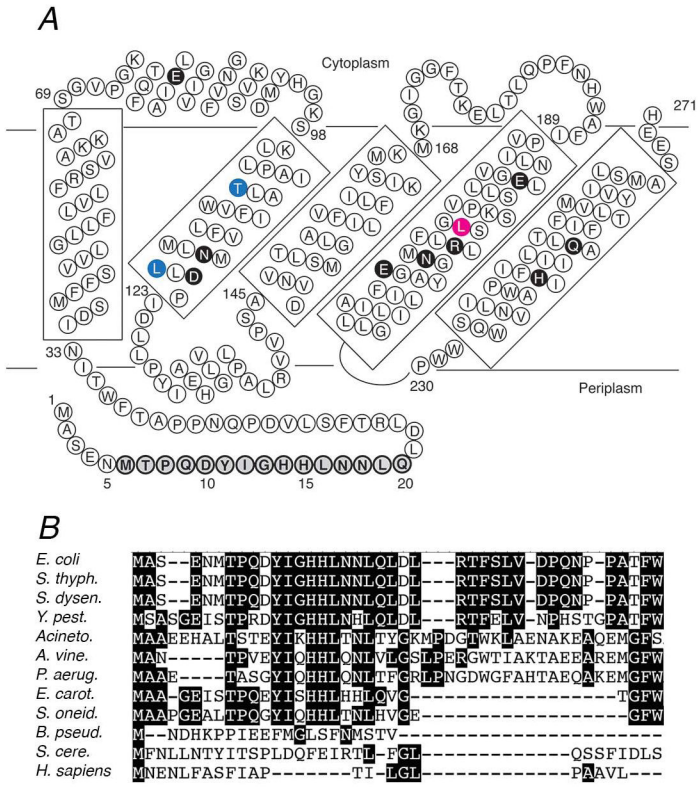

Fig. 1.

Amino acid sequence of subunit *a* from *E. coli*. ***A*** A membrane topology model of subunit *a*. The residues near the N-terminus that have been deleted in this study are shaded gray with a bold circle. Seven of these residues are strictly conserved among the first 9 species listed in panel *B*. Residues that are possibly functional in proton translocation, or subunit interactions, are shaded black. Two residues that have been cross-linked to subunit *b* (DeLeon-Rangel et al. 2013), and are used in this study, Thr 107 and Leu 121, are colored blue. A residue that has been cross-linked to subunit *c* (Jiang and Fillingame 1998), and is used in this study, Leu 207, is colored magenta. ***B*** Sequence comparison of the N-terminal region of subunit *a* from 10 bacterial species, and from the ATP6 protein of yeast and human mitochondria. The strictly conserved residues are portrayed as white text on black background. The species listed (and the accession codes) are given: *Escherichia coli* (NC_000913), *Salmonella typhimurium* LT2 (NC_003197), *Shigella dysenteriae* Sd197 (NC_007606), *Yersinia pestis* CO92 (NC_003143), *Acinetobacter* sp. ADP1 (NC_005966), *Azotobacter vinelandii* DJ (NC_012560), *Pseudomonas aeruginosa* PAO1 (NC_002516), *Erwinia carotovora* subsp. Atroseptica (NC_004547), *Shewanella oneidensis* MR-1 (NC_004347), *Bacillus pseudofirmus* OF4 (NC_013791), *Saccharomyces cerevisiae* (NP_009313.1), *Homo sapiens* (YP_003024031). Alternative alignments of the mitochondrial sequences have been published recently (Hahn et al. 2016; Morales-Rios et al. 2015)

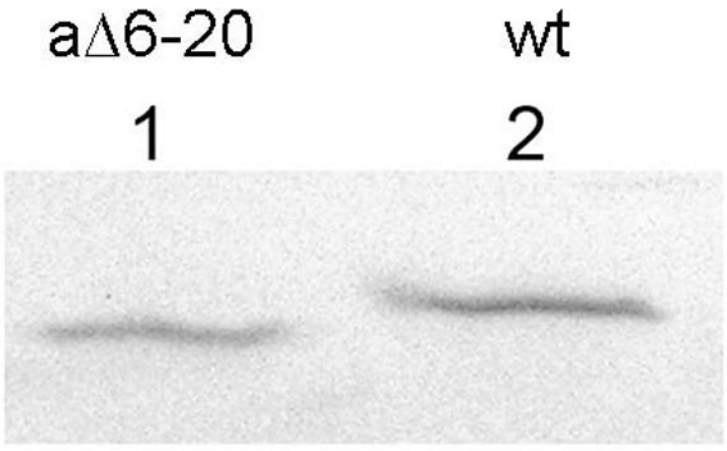

Fig. 2.

Immunoblot of truncated subunit *a* from membrane vesicle preparations. Membrane vesicles were prepared from cells as described in “Materials and methods”. 40 μg membrane protein were loaded in each lane. The blot was probed with anti-HA antibody. Lane 1, RH305/pIRR2-HisHA-*a*Δ6–20 (truncated subunit *a*). Lane 2, RH305/pIRR2-HisHA (full length subunit *a*)

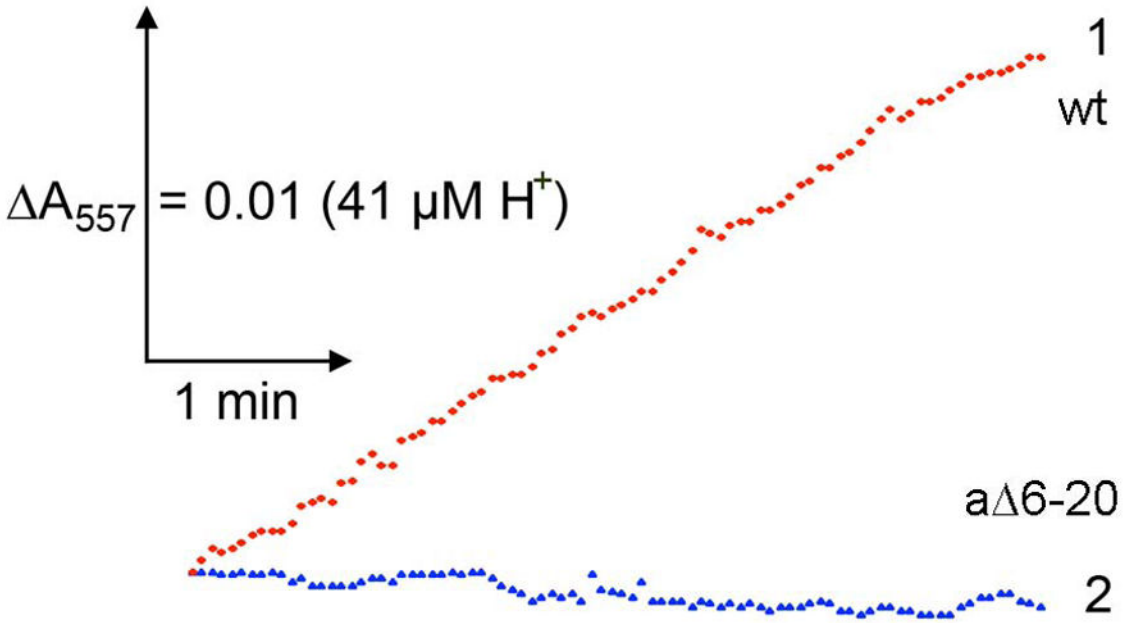

Fig. 3.

ATP synthesis by membrane vesicles. ATP synthesis was measured by the phenol red assay at 557 nm (Chance and Nishimura 1967; Ishmukhametov et al. 2005; Zharova and Vinogradov 2006). The reactions were initiated by the addition of 20 mM succinate. Trace 1, wild type membranes (DK8/pFV2). Trace 2, DK8/pFV2-*a*Δ6–20. The assay contained 200 μg membrane protein per reaction (2 mL). Representative traces are shown. Similar results have been obtained using a luciferase assay (Galkin et al. 2006)

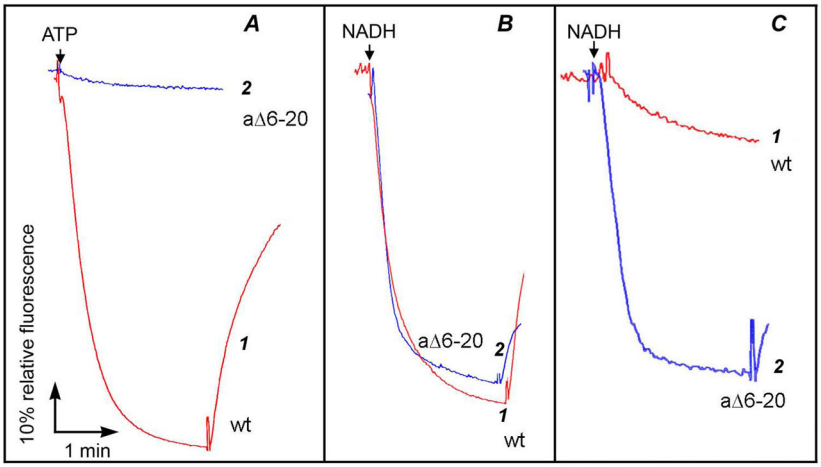

Fig. 4.

Proton translocation by membrane vesicles. Rates of proton translocation are estimated from the rates of fluorescence quenching of the acridine dye ACMA. In each case 40 μg of membrane protein was added to the assay chamber of 2 mL. In each panel trace 1 represents wild type membranes (DK8/pFV2) and trace 2, DK8/pFV2-*a*Δ6–20. ***A*** ATP-driven proton translocation by membrane vesicles, using 0.20 mM ATP. ***B*** NADH-driven proton translocation by membrane vesicles, using 0.20 mM NADH. ***C*** NADH-driven proton translocation by membranes stripped of F_1-ATPase, using 0.20 mM NADH. Stripped membranes are permeable to protons if the F_o is functional

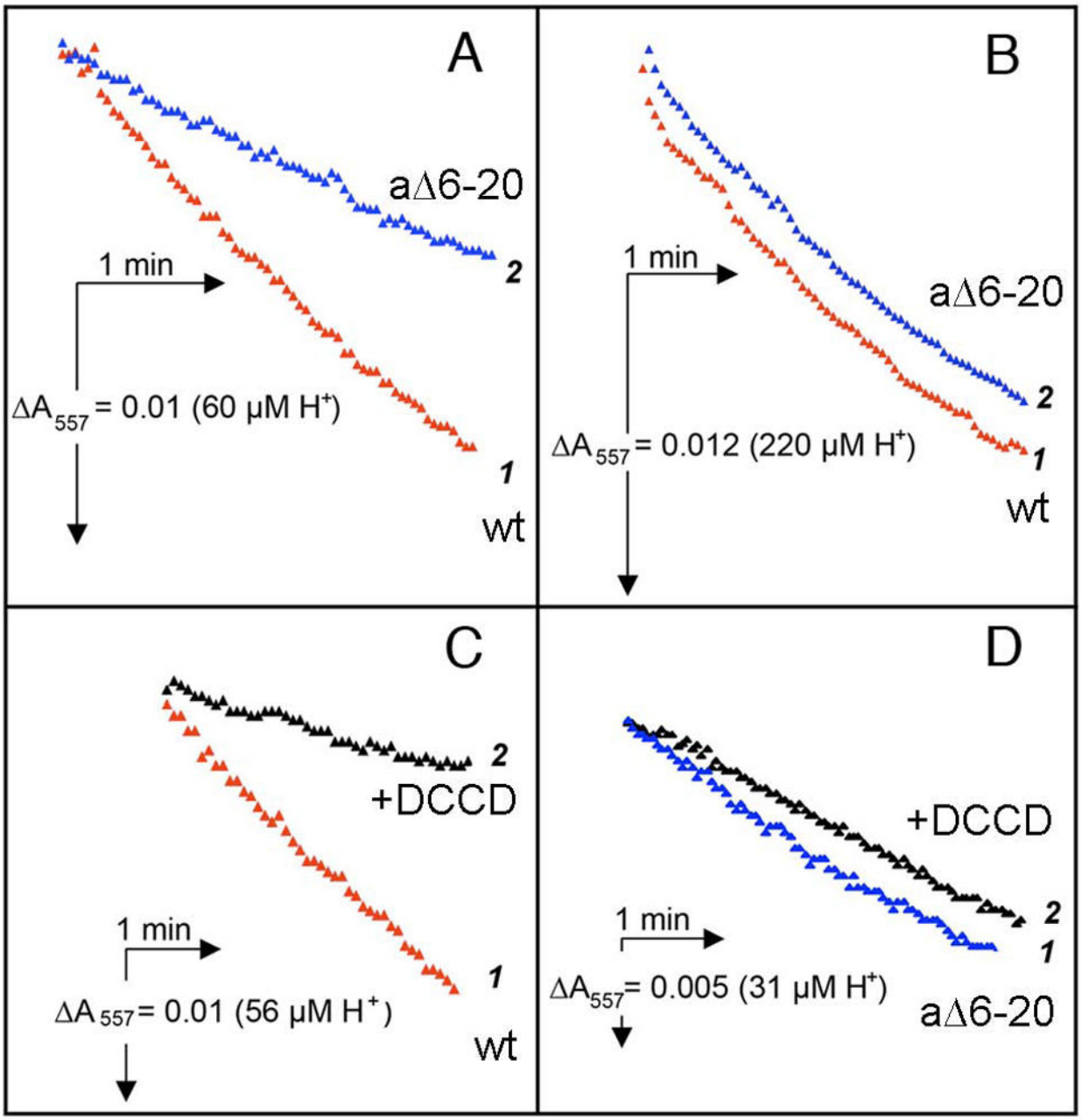

Fig. 5.

ATP hydrolysis rates by membrane vesicles. Representative traces are shown for assays at 37°C and 1 mM ATP. ***A*** Rates of ATP hydrolysis of the wild type, DK8/pFV2, (trace 1, 0.32 units/mg protein) and DK8/pFV2-*a*Δ6–20 (trace 2, 0.145 units/mg protein) are shown as measured by the phenol red assay. ***B*** ATP hydrolysis rates are measured as in panel A, with the addition of 0.4 % LDAO. The two rates are about 0.88 units/mg. ***C*** The rates of ATP hydrolysis of the wild type membranes are measured without (trace 1) or with (trace 2) a pre-treatment of 50 μM DCCD. ***D*** The rates of ATP hydrolysis of DK8/pFV2-*a*Δ6–20

membranes are measured without (trace 1) or with (trace 2) a pre-treatment of 50 μM DCCD. In all panels representative traces are shown

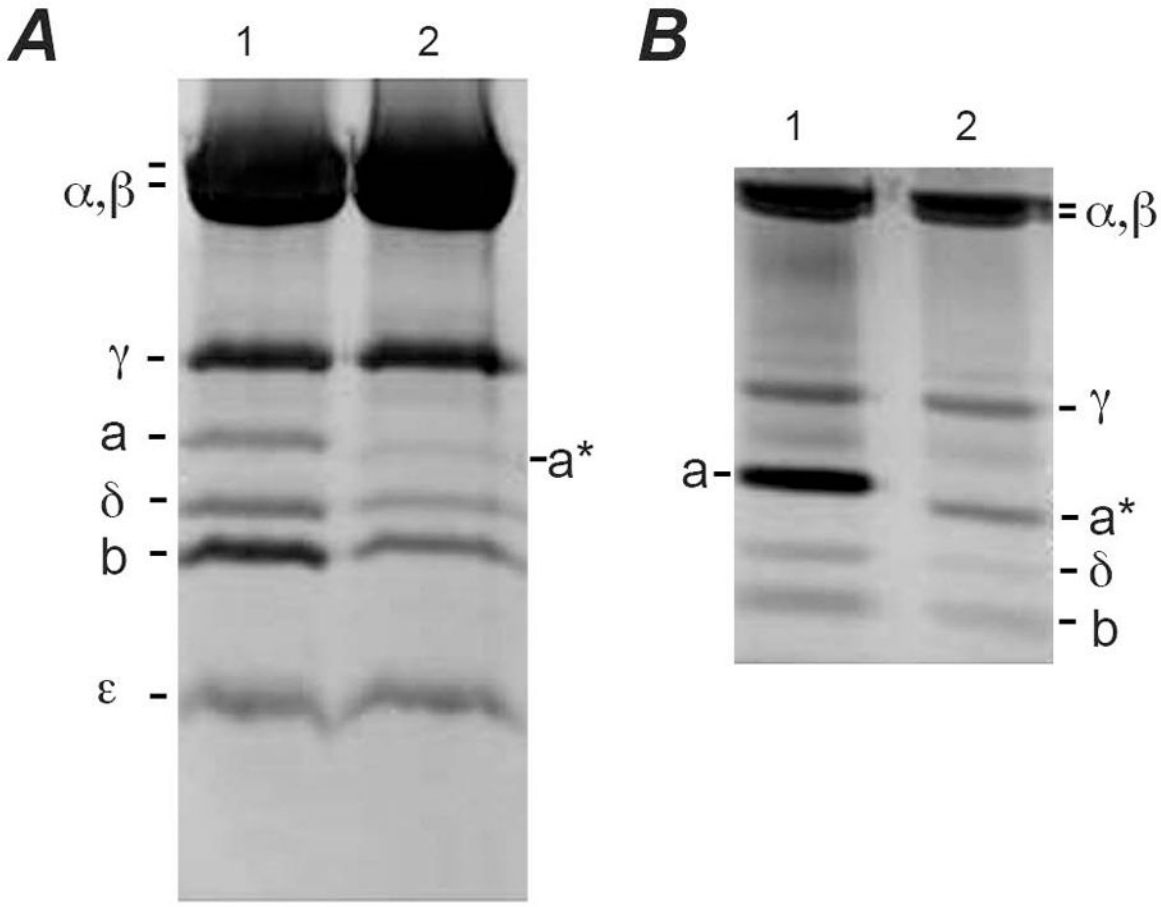

Fig. 6.

Subunit composition of the isolated ATP synthase from wild type DK8/pFV2 and from DK8/pFV2-*a*Δ6–20. ***A*** Coomassie Blue stained gel with 20 μg protein loaded per lane. ***B*** Silver-stained gel with 10 μg protein loaded per lane. In each panel lane 1 is the wild type enzyme, and trace 2 is from the *a*Δ6–20 strain. The location of the truncated subunit *a* is indicated by a*. Subunit *a* stains strongly with silver, but weakly with Coomassie Blue due to its hydrophobicity. The bottoms of the gels are not shown, omitting *c* subunits in panel A, and epsilon and *c* subunits in panel B

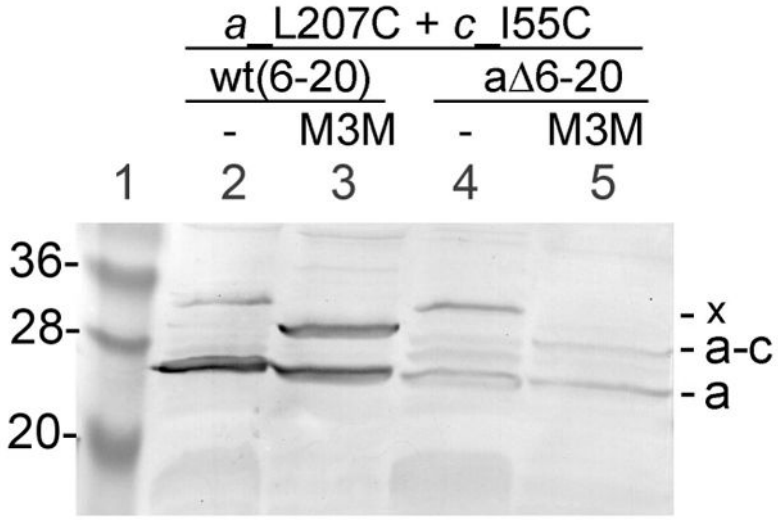

Fig. 7.

Cross-linking of subunits *a* and *c* in membrane vesicles. Mutations *a*_L207C and *c*_I55C were constructed in the background of the wild type enzyme, pFV2-HA, and in the truncated subunit *a*, pFV2-HA *a*Δ6–20. Membrane vesicles were prepared from both strains, and treated with M3M to promote cross-linking. An immunoblot using anti-HA to detect subunit *a* is shown. Equal amounts of protein were loaded in each lane. Lane 1, pre-stained protein standards, 20, 28, and 36 kilodaltons. Lane 2, *a*_L207C and *c*_I55C in the wild type background, untreated. Lane 3, *a*_L207C and *c*_I55C in the wild type background, treated with M3M. Lane 4, *a*_L207C and *c*_I55C in the truncated subunit *a* (DK8/pFV2-*a*Δ6–20) background, untreated. Lane 5, *a*_L207C and *c*_I55C in the truncated subunit *a* (DK8/pFV2-*a*Δ6–20) background, treated with M3M. The migration of subunit *a* and the *a*-*c* covalent cross-link are indicated at the right. The upper band marked by an *x* is an artifact

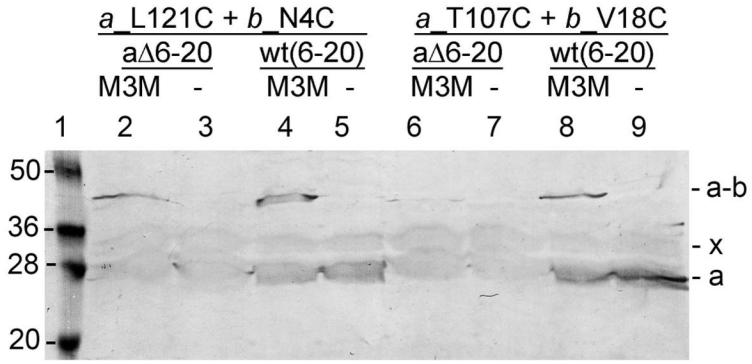

Fig. 8.

Cross-linking of subunits *a* and *b* in membrane vesicles. Mutations *a*_L121C + *b*_N4C and *a*_T107C + *b*_V18C were constructed in the background of the wild type enzyme, pFV2-HA, and in the truncated subunit *a*, pFV2-HA *a*Δ6–20. Membrane vesicles were prepared from both strains, and treated with M3M to promote cross-linking. An immunoblot using anti-HA to detect subunit *a* is shown. Equal amounts of protein were loaded in each lane. Lane 1, pre-stained protein standards, 20, 28, 36, and 50 kilodaltons. Lane 2, *a*_L121C + *b*_N4C in pFV2-HA *a*Δ6–20, treated with M3M. Lane 3, *a*_L121C + *b*_N4C in pFV2-HA *a*Δ6–20, untreated. Lane 4, *a*_L121C + *b*_N4C in wild type pFV2-HA, treated with M3M. Lane 5, *a*_L121C + *b*_N4C in wild type pFV2-HA, untreated. Lane 6, *a*_T107C and *b*_V18C in pFV2-HA *a*Δ6–20, treated with M3M. Lane 7, *a*_T107C and *b*_V18C in pFV2-HA *a*Δ6–20, untreated. Lane 8, *a*_T107C and *b*_V18C in wild type pFV2-HA, treated with M3M. Lane 9, *a*_T107C and *b*_V18C in wild type pFV2-HA, untreated. The migration of subunit *a* and the *a*-*b* covalent cross-link are indicated at the right. The diffuse band just above the band for subunit *a*, and marked by an x, is an artifact

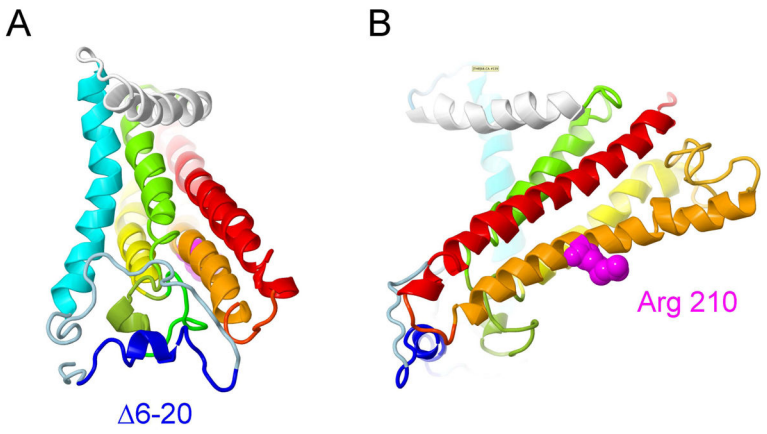

Fig. 9.

View of the homology model of subunit a based on the bovine mitochondrial enzyme. The following coloring scheme is used: N-terminus is light blue, with the deleted residues in dark blue, H1 is cyan, the cytoplasmic H2 is white, H3 is green, H4 is yellow, H5 is orange, and H6 is red. ***A*** Subunit *a* is oriented with the cytoplasm at the top, and the periplasm at the bottom. The deleted residues, 6–20, colored blue, are at the periplasmic surface. H1-H3 are in the front of the view. ***B*** This view is rotated 90° from the previous panel. The key residue, Arg 210, is shown in space filling, colored magenta. H5 and H6 are in the front of the view, and they form the primary contact with the ring of *c* subunits